J. Meas. Sci. Instrum., 2025, 16(4): 558-568. http://jmsi.publish.founderss.cn
DOI: 10.62756/jmsi.1674-8042.2025054 jmsi@nuc.edu.cn

Homography matrix estimation method based on adaptive genetic algorithm

QIAN Cheng, ZHU Zhifeng*, YANG Ke, ZHANG Tao, JI Guotai

Anhui Provincial Key Laboratory of Power Electronics and Motion Control, Anhui University of Technology, Ma'anshan 243000, China

***Corresponding author:** ZHU Zhifeng (zzf@ahut.edu.cn)

Received: May 28, 2025 **Revised:** July 16, 2025 **Accepted:** August 23, 2025

Abstract: In camera calibration, accurate estimation of homography matrix between the world coordinates of the calibration board and its image coordinates is a key step in high-precision calibration of intrinsic camera parameters. The existing homography matrix estimation methods have problems such as dependence on thresholds, low computational efficiency, and initial model or sorting quality affecting results. In this paper, a homography matrix estimation method based on adaptive genetic algorithm was proposed. Firstly, a new circular grid calibration board was designed and the strategy of first sampling of data sets was optimized. Secondly, a mathematical model for the estimated homography matrix was established according to the adaptive genetic algorithm. Thereby the optimal homography matrix between the calibration board and its image was obtained. Finally, the intrinsic camera parameters were calculated based on Zhang's calibration method. The experimental results show that compared with the results of three traditional estimation methods RANSAC, PROSAC, and LMEDS, the reprojection error of the images by our estimation method is reduced by about 4.11%—7.85%, 11.94%—16.91%, and 10.19%—17.82%, respectively; and the average running time of the algorithm decreases by about 25.85%—37.47%, 11.99%—22.71%, and 46.50%—53.35%, respectively. In addition, the homography matrix estimation method in this paper was applied to camera calibration. The results show that compared with the traditional estimation method, the average accuracy of the camera during the calibration process increases by about 5.48%, 15.06%, and 11.47%, respectively; and the average calibration efficiency of the camera is improved by about 10.13%, 5.71%, and 14.26%, respectively. The homography matrix estimation method proposed in this paper not only obtained reliable results, but also had certain value and significance in improving the estimation accuracy and calculation efficiency in camera calibration.

Key words: camera calibration; intrinsic camera parameters; calibration board; homography matrix; reprojection error; Zhang's calibration

0 Introduction

Camera calibration directly affects the accuracy and reliability of subsequent image processing and analysis[1,2]. However, due to changes in the lighting environment or differences in camera angles[3], when some key points are detected, there may be a certain degree of positioning error, which leads to some matching point pairs[4,5] of low quality in the data set, and thus adversely affects the solution of the homologous matrix[6].

To avoid this problem, some researchers proposed robust estimation algorithms such as RANSAC[7], PROSAC[8], and LMedS[9]. The RANSAC algorithm estimates the homography matrix by randomly selecting minimal sample sets, then computes the projection errors between all other matching point pairs and the model, classifying them as inliers or outliers based on a predefined threshold. The algorithm requires multiple iterations to obtain the best model, resulting in high computational costs and significantly affected by threshold selection. The PROSAC algorithm is an improvement of the RANSAC algorithm, which reduces the computational effort by selecting new samples from pairs of points with smaller errors after each iteration rather than completely random selection. But when the initial model estimate is inaccurate or the proportion of inlier points in the dataset is low, this algorithm may not ensure the accuracy of the final model. The LMedS algorithm finds the best model by minimizing the median error of matching point pairs, effectively avoiding the impact of the existence of numerous abnormal matching point pairs on the estimation results. However, this method requires sorting the errors of all matching point pairs, which improves the computational complexity. In addition, using median error as a standard may not fully reflect the best fit of the model, especially when there are many

useful matching point pairs in the dataset. LMedS may not be able to make full use of this information, resulting in the model estimation being impossible to achieve optimality.

In recent years, many researchers improved these robust algorithms or proposed some new homography matrix estimation methods. Lai et al.[10] proposed an improved RANSAC algorithm for estimating homography matrix. A priori probability sampling method was used instead of the random sampling method, and a quadratic matching strategy was introduced into calculation of the matching error, to eliminate more mismatched point pairs, thereby to improve the accuracy of the homography matrix. However, the prior probability depends on the distance measurement of the key points, making this method unsuitable for all image scenarios, and the results are greatly affected by the error of the key point extraction. Zhao et al.[11] used the HALF-SIFT method to compensate for the positioning errors generated during feature extraction, and adopted a new internal point selection method and homography matrix refinement method: covariance weighted[12] MLESAC[13] and covariance weighted L-M[14]. This method improves the accuracy and robustness of homography matrix estimation by taking into account the anisotropy and inhomogeneity of feature positioning errors. Therefore, this method has high computational complexity and the calculation amount of the algorithm is relatively large. Yan et al.[15] proposed an unsupervised depth homography method. This method designed a multi-scale feature pyramid twin network to extract multi-scale feature information of images, and combined dynamic attention mechanism[16] and deep learning technology[17] to effectively solve the homography problem in repetitive texture scenarios. Nevertheless, this method requires the construction of a complex model and numerous resources to train the model, resulting in high cost of algorithm implementation.

In this paper, a novel and efficient homography matrix estimation method was proposed to optimize the homography matrix estimation of calibration board and its images with Zhang's camera calibration method. Firstly, a new circular grid calibration board was designed to adapt to the iterative calculation of subsequent genetic algorithms. Next, the strategy for matching points to initially sample the data set was optimized. Then, an adaptive genetic algorithm was introduced to establish a mathematical model that estimates the optimal homography matrix of the calibration board and its image. Experimental results showed that compared with the traditional estimation methods namely RANSAC, PROSAC, and LMedS, the homography matrix estimated by adaptive genetic algorithm not only significantly reduced the reprojection error of the image, but also reduced the average running time of the algorithm. At the same time, this method also effectively improved the estimation accuracy and calibration efficiency during the camera calibration process.

1 Camera calibration mathematical model

1.1 Perspective projection imaging process

In order to describe the imaging process of objects from three-dimensional space mapped to two-dimensional planes, a mathematical model of the process of object perspective projection imaging[18,19] is established, as shown in Fig.1.

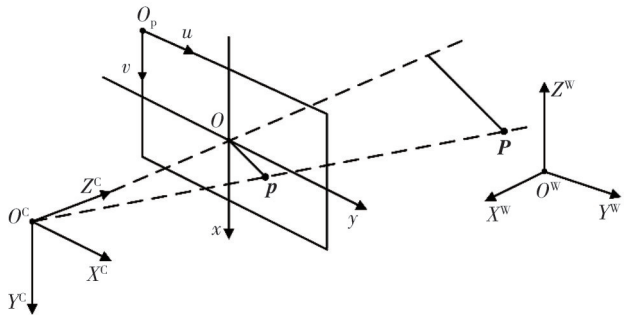

Fig. 1 Object perspective projection imaging model

According to the projection imaging model, the coordinates of the target point $\boldsymbol{P}$ in three-dimensional space need to be converted from the world coordinate system to the camera coordinate system by rotation and translation. According to the principle of similarity transformation, the corresponding imaging point $\boldsymbol{p}$ of the target point in the image coordinate system can be obtained. Then, combining the width and height information of the pixel on the physical size, the coordinates of the imaging point are further converted from the image coordinate system to the pixel coordinate system. This conversion process[20] is

$$s\begin{bmatrix} u_p \\ v_p \\ 1 \end{bmatrix} = \boldsymbol{K}\left[\boldsymbol{R}|\boldsymbol{t}\right]\begin{bmatrix} X_P^W \\ Y_P^W \\ Z_P^W \\ 1 \end{bmatrix} = \begin{bmatrix} f_x & \alpha & u_0 \\ 0 & f_y & v_0 \\ 0 & 0 & 1 \end{bmatrix}\begin{bmatrix} r_{11} & r_{12} & r_{13} & t_1 \\ r_{21} & r_{22} & r_{23} & t_2 \\ r_{31} & r_{32} & r_{33} & t_3 \end{bmatrix}\begin{bmatrix} X_P^W \\ Y_P^W \\ Z_P^W \\ 1 \end{bmatrix}, \tag{1}$$

where s is the scale factor, $\begin{bmatrix} u_p & v_p & 1 \end{bmatrix}^{\mathrm{T}}$ represents the

coordinates of the imaging point $\boldsymbol{p}$ in the pixel coordinate system, $\begin{bmatrix} X_P^{\mathrm{W}} & Y_P^{\mathrm{W}} & Z_P^{\mathrm{W}} & 1 \end{bmatrix}^{\mathrm{T}}$ represents the coordinates of the target point $\boldsymbol{P}$ in the world coordinate system, $\boldsymbol{K}$ is the camera internal parameter matrix, and $[\boldsymbol{R}|\boldsymbol{t}]$ is the external parameter matrix.

1.2 Homography matrix of calibration board and its image

The calibration board plane is used as the xoy reference plane, and the z axis is perpendicular to the calibration board plane to establish a world coordinate system. Then the reflective mark on the calibration board can be considered to lie on the same plane with $Z_P^{\mathrm{W}}=0$. Therefore, there is a homographic relationship[21] between the real plane of the calibration board and its image plane. This relationship can be represented by a homography matrix, and the specific form is

$$s\begin{bmatrix} u_p \\ v_p \\ 1 \end{bmatrix}=\begin{bmatrix} h_{11} & h_{12} & h_{13} \\ h_{21} & h_{22} & h_{23} \\ h_{31} & h_{32} & h_{33} \end{bmatrix}\begin{bmatrix} X_P^{\mathrm{W}} \\ Y_P^{\mathrm{W}} \\ 1 \end{bmatrix}, \tag{2}$$

where s is the scale factor, the first matrix to the right of the equation is a homography matrix, represented by $\boldsymbol{H}$. By expanding the matrix into equation form, the linear equations can be obtained by

$$\begin{cases} u_p=\dfrac{h_{11}X_P^{\mathrm{W}}+h_{12}Y_P^{\mathrm{W}}+h_{13}}{h_{31}X_P^{\mathrm{W}}+h_{32}Y_P^{\mathrm{W}}+h_{33}}, \\ v_p=\dfrac{h_{21}X_P^{\mathrm{W}}+h_{22}Y_P^{\mathrm{W}}+h_{23}}{h_{31}X_P^{\mathrm{W}}+h_{32}Y_P^{\mathrm{W}}+h_{33}}. \end{cases} \tag{3}$$

It follows that two linear equations are obtained by a set of corresponding points. In addition, according to the scale-invariant property of the homogeneous coordinates, $\boldsymbol{H}$ is multiplied by any non-zero constant k. Although there are changes in terms of scale, the equation still holds. Let $k=1/h_{33}$, there is

$$\boldsymbol{H}'=\frac{1}{h_{33}}\boldsymbol{H}=\begin{bmatrix} h'_{11} & h'_{12} & h'_{13} \\ h'_{21} & h'_{22} & h'_{23} \\ h'_{31} & h'_{32} & 1 \end{bmatrix}. \tag{4}$$

It follows that the homography matrix has 8 degrees of freedom. Combined with Eq. (3), it can be seen that at least 4 sets of corresponding points are required to calculate the homography matrix $\boldsymbol{H}$. Assume that there are 4 sets of corresponding points, the solution to homography is expressed as

$$\begin{bmatrix} X_1^{\mathrm{W}} & Y_1^{\mathrm{W}} & 1 & 0 & 0 & 0 & -u_1X_1^{\mathrm{W}} & -u_1Y_1^{\mathrm{W}} & -u_1 \\ 0 & 0 & 0 & X_1^{\mathrm{W}} & Y_1^{\mathrm{W}} & 1 & -v_1X_1^{\mathrm{W}} & -v_1Y_1^{\mathrm{W}} & -v_1 \\ \vdots & \vdots & \vdots & \vdots & \vdots & \vdots & \vdots & \vdots & \vdots \\ X_4^{\mathrm{W}} & Y_4^{\mathrm{W}} & 1 & 0 & 0 & 0 & -u_4X_4^{\mathrm{W}} & -u_4Y_4^{\mathrm{W}} & -u_4 \\ 0 & 0 & 0 & X_4^{\mathrm{W}} & Y_4^{\mathrm{W}} & 1 & -v_4X_4^{\mathrm{W}} & -v_4Y_4^{\mathrm{W}} & -v_4 \end{bmatrix}\begin{bmatrix} h_{11} \\ h_{12} \\ h_{13} \\ h_{21} \\ h_{22} \\ h_{23} \\ h_{31} \\ h_{32} \\ h_{33} \end{bmatrix}=0, \tag{5}$$

where $i=1,2,3,4$ respectively represents the sequence numbers of the four corresponding points, and the pixel coordinates and plane coordinates are represented by $(u_i,v_i,1)^{\mathrm{T}}$ and $(X_i^{\mathrm{W}},Y_i^{\mathrm{W}},1)^{\mathrm{T}}$ respectively.

1.3 Solving camera parameters in homography matrix

When the camera is fixed, and the calibration board is placed at different positions within the camera's field of view, the images from multiple perspectives can be captured to obtain rich geometric information. According to Section 1.2, there is a homography matrix $\boldsymbol{H}$ between each image and the calibration board plane. With Eqs. (1) and (2), it can be seen that when $Z_P^{\mathrm{W}}=0$ in the world coordinate system, the parameters matrix $\boldsymbol{K}$ in the camera, the column vectors $\boldsymbol{r}_1$ and $\boldsymbol{r}_2$ of the rotation matrix $\boldsymbol{R}$, and the translation matrix $\boldsymbol{t}$ have a relationship with the homologous matrix as shown in

$$\boldsymbol{H}=\lambda\boldsymbol{K}\begin{bmatrix} \boldsymbol{r}_1 & \boldsymbol{r}_2 & \boldsymbol{t} \end{bmatrix}, \tag{6}$$

where λ is the scale factor. If the $\boldsymbol{H}$ matrix is expressed in the form of column vectors as $\begin{bmatrix} \boldsymbol{h}_1 & \boldsymbol{h}_2 & \boldsymbol{h}_3 \end{bmatrix}$, then we can obtain

$$\begin{cases} \boldsymbol{r}_1=\lambda^{-1}\boldsymbol{K}^{-1}\boldsymbol{h}_1, \\ \boldsymbol{r}_2=\lambda^{-1}\boldsymbol{K}^{-1}\boldsymbol{h}_2, \\ \boldsymbol{t}=\lambda^{-1}\boldsymbol{K}^{-1}\boldsymbol{h}_3. \end{cases} \tag{7}$$

At the same time, the rotation matrix $\boldsymbol{R}$ has the characteristics that all column vectors are unit vectors and any two column vectors are orthogonal, that is, $\boldsymbol{r}_1^{\mathrm{T}}\boldsymbol{r}_2=0$, $\boldsymbol{r}_1^{\mathrm{T}}\boldsymbol{r}_1=\boldsymbol{r}_2^{\mathrm{T}}\boldsymbol{r}_2$. Combined with Eq. (7), two constraints for camera internal parameters can be derived as

$$\begin{cases} \boldsymbol{h}_1^{\mathrm{T}}(\boldsymbol{K}^{-1})^{\mathrm{T}}\boldsymbol{K}^{-1}\boldsymbol{h}_2=0, \\ \boldsymbol{h}_1^{\mathrm{T}}(\boldsymbol{K}^{-1})^{\mathrm{T}}\boldsymbol{K}^{-1}\boldsymbol{h}_1-\boldsymbol{h}_2^{\mathrm{T}}(\boldsymbol{K}^{-1})^{\mathrm{T}}\boldsymbol{K}^{-1}\boldsymbol{h}_2=0. \end{cases} \tag{8}$$

Let $\boldsymbol{B}=\mu(\boldsymbol{K}^{-1})^{\mathrm{T}}\boldsymbol{K}^{-1}$, and it can be seen that $\boldsymbol{B}$ is a

symmetric matrix with 6 unknown elements. Therefore, solving it requires at least calibration of the homography matrix between the calibration board plane and the 3 images. If matrix $\boldsymbol{B}$ is known, the camera internal parameters can be further derived as

$$\begin{cases} v_0=(B_{12}B_{13}-B_{11}B_{23})/(B_{11}B_{22}-B_{12}^2), \\ \mu=B_{33}-\left[B_{13}^2+v_0(B_{12}B_{13}-B_{11}B_{23})\right]/B_{11}, \\ f_x=\sqrt{\mu/B_{11}}, \\ f_y=\sqrt{\mu B_{11}/(B_{11}B_{22}-B_{12}^2)}, \\ \alpha=-B_{12}f_x^2 f_y/\mu, \\ u_0=\alpha v_0/f_y-B_{13}f_x^2/\mu. \end{cases} \tag{9}$$

2 Homography matrix estimation method

In this paper, the implementation of the homography matrix estimation method is mainly divided into two parts. The first part is to design a new calibration board and optimize the initial sampling strategy of matching points to the data set. The second part, based on the matching point pairing data set, the evolutionary idea of adaptive genetic algorithm is introduced to estimate the optimal homography matrix, thereby improving the accuracy and efficiency of homography estimation.

2.1 Design and sampling strategy of new calibration board

Traditional calibration boards have two types: checkerboard grid and circular grid, as shown in Fig.2. The black and white grids on the checkerboard grid plane are clearly separated, and the positions of key points can be accurately identified, which has the advantage of high recognition accuracy. However, it is more sensitive to light changes, and the detection of key points is greatly affected in strong light reflections or uneven light environments. In contrast, circular grid usually exhibits better geometric stability in camera imaging. Even if there is occlusion or ambient light changes, the center of the reflective mark as a key point can still be easily detected at different angles. However, due to the neat and symmetrical arrangement of the reflective marks on the traditional circular grid calibration board, the calibration board lacks directionality, and can't provide a clear directional reference for the camera during the calibration process. In addition, when 4 points are selected, four points are easily collinear, and the $\boldsymbol{H}$ matrix can't be accurately solved. Besides, recent studies also proposed the use of absolute phase targets[22,23], as shown in Fig.2(c). Nevertheless, using absolute phase targets usually requires additional hardware support (such as projectors, encoding modules, etc.), and requires the projection system to be accurately synchronized with the camera's shooting, which makes the system integration complexity. Therefore, this paper finally chooses to improve the traditional circular grid calibration board, as shown in Fig.2(d). The reflective marks on the calibration board are distributed asymmetrically, and the plane of the calibration board is divided into four areas, and the reflective marks in each area form a triangle shape, which can make it clear directionality for shooting at any angle of view. At the same time, when there are enough reflective marks on the calibration board, this asymmetric design can significantly reduce the situation that the four reflective marks on the plane are collinear, effectively improve the effectiveness and efficiency of the calculation.

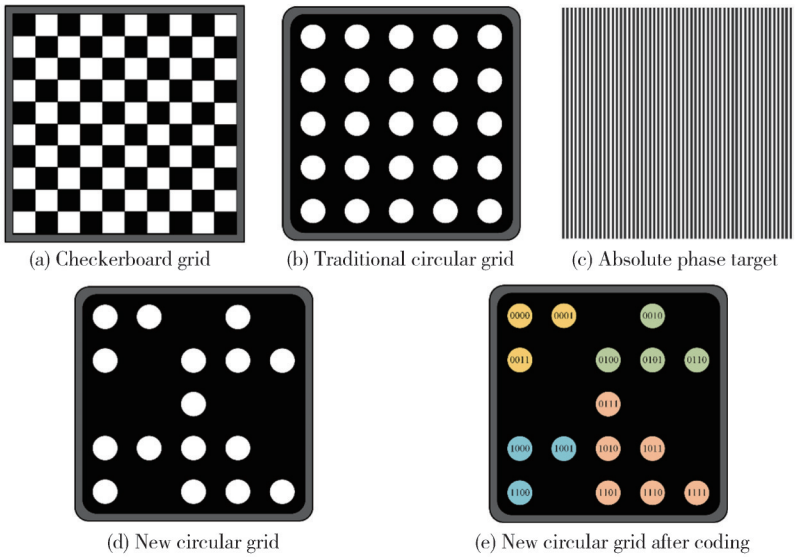

(a) Checkerboard grid (b) Traditional circular grid (c) Absolute phase target

(d) New circular grid (e) New circular grid after coding

Fig. 2 Calibration boards

The solution of the homography matrix needs to select 4 point pairs from the matched point pair data set for direct linear transformation calculation. Whether using RANSAC, LMedS, or other algorithms, there is often a problem of initial sampling. At present, the initial sampling strategy of most algorithms adopts a random method, but in some algorithms, the random method of initial sampling might directly affect the final model results. Therefore, this paper optimizes the initial sampling strategy of the adaptive genetic algorithm and abandons the traditional random sampling method. First, the matched point pair data set is grouped according to the four regions of the calibration board plane. Second, a matching point pair is randomly selected from each of the four groups. In the process of generating the initial chromosome ancestral population of the adaptive genetic algorithm, the use of such an initial sampling strategy can make the initial population diverse, which helps the algorithm to explore widely in the search space and avoids falling into the local optimal solution, thereby effectively improving the computational efficiency and accuracy of homography estimation.

2.2 Estimating homography matrix based on adaptive genetic algorithm

If there are N sets of corresponding points between the calibration board and its image, these N sets of corresponding points can constitute a matching point pair data set. Based on this data set, some algorithms can be used to estimate the optimal homography matrix. Among them, RANSAC, PROSAC, and LMedS are several classic algorithms. However, these algorithms usually have shortcomings of large number of iterations and large amount of computation. At the same time, parameter thresholds often need to be set based on experience, and the performance of the final model may be significantly affected by the initial model. Therefore, this paper proposed a method based on adaptive genetic algorithm[24,25] to estimate the optimal homography matrix between the calibration board and its image. This method simulates the evolution process in nature to quickly and accurately estimate the optimal homography matrix. The specific algorithm steps are as follows:

Step 1 The reflective mark is encoded on the new calibration board. The encoding method is binary, and the encoding order follows the principle of from left to right and from top to bottom. The reflective marks on the target board are numbered 0000B—1111B, which is also used as the point pair number between the reflective marks on the calibration board and the corresponding points of their images, as shown in Fig.2(e).

Step 2 Matching point pair dataset D is constructed. The calibration board image is captured by a camera. After preprocessing, the calibration board image is fitted with an ellipse using the least squares method to extract the center coordinates of all reflective marks in the image. The center coordinates are matched with the plane coordinates of the reflective marks to obtain the matching point pair dataset D.

Step 3 In initial stage, chromosome ancestral population is generated. According to the optimized initial sampling strategy, 6 matching point pair sequences from data set D are generated to form a chromosome ancestral population F. Each matching point pair sequence is a chromosome, which consists of 4 matching point pairs. Each matching point pair can be regarded as a gene unit on the chromosome. The generated chromosome ancestral population F is shown in Fig.3. Each gene unit represents a matching point pair. It is represented by four small squares of binary 0 or 1, which is the basis for subsequent chromosome crossing or mutation. In the initial stage, different colored blocks are used to indicate that the gene units come from different areas of the calibration board. After this, the changes in the color blocks are used to demonstrate the process of chromosome crossover or mutation.

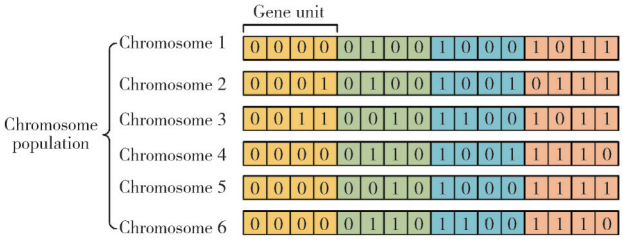

Fig. 3 Chromosome ancestral population F

Step 4 The probability of chromosome crossover and mutation is adaptively adjusted. In order to find the optimal solution globally, it is stipulated that the chromosomes with lower fitness have greater possibility of crossover and mutation, to ensure that the iterative results will gradually approach the optimal solution. During the crossover process, the crossover probability formula of two chromosomes is expressed as

$$Pr_{\mathrm{c}}=\begin{cases} Pr_{\mathrm{cMIN}}, & f'\geqslant f_{\mathrm{avg}}, \\ Pr_{\mathrm{cMAX}}-(Pr_{\mathrm{cMAX}}-Pr_{\mathrm{cMIN}})\times\dfrac{f'-f_{\mathrm{MIN}}}{f_{\mathrm{avg}}-f_{\mathrm{MIN}}}, & f'<f_{\mathrm{avg}}, \end{cases} \tag{10}$$

where f_{MIN} is the minimum fitness value in the population; f_{avg} is the average fitness of the population; f'

is the fitness value of the chromosome with the smaller fitness; Pr_{cMAX} and Pr_{cMIN} are the maximum and minimum values of the crossover probability. During the mutation process, the mutation probability formula of chromosomes is expressed as

$$Pr_{\mathrm{m}}=\begin{cases} Pr_{\mathrm{mMIN}}, & f\geqslant f_{\mathrm{avg}}, \\ Pr_{\mathrm{mMAX}}-(Pr_{\mathrm{mMAX}}-Pr_{\mathrm{mMIN}})\times\dfrac{f-f_{\mathrm{MIN}}}{f_{\mathrm{avg}}-f_{\mathrm{MIN}}}, & f<f_{\mathrm{avg}}, \end{cases} \tag{11}$$

where f_{MIN} is the minimum fitness value in the population; f_{avg} is the average fitness of the population; f is the fitness value of the chromosome; Pr_{mMAX} and Pr_{mMIN} are the maximum and minimum values of the mutation probability.

Step 5 A new chromosome population is generated. The gene crossover or mutation operations on the chromosome ancestral population are performed to generate a new chromosome population S. The process of chromosome gene crossover and mutation is shown in Fig. 4. In the process of crossing two chromosomes, gene fragments with equal numbers and the same size are randomly selected for crossover operations. In the process of mutation of one chromosome, the bit of the gene unit randomly generates a mutation operation, changing the binary bit from 0 to 1, or from 1 to 0.

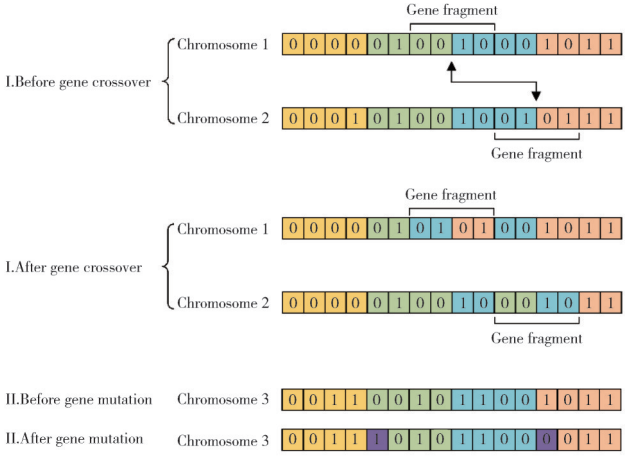

Fig. 4 Chromosome gene crossover and mutation

Step 6 According to Eq. (5), the homography matrix $\boldsymbol{H}$, corresponding to all chromosomes in the chromosome ancestral population F and the newly generated chromosome population S is calculated. In addition, the root mean square error is evaluated as a fitness function for each chromosome in the population. We sort their fitness and select the 6 chromosomes with low fitness as the winners of this evolution, and use them to replace the previous ancestral population F. Here, it is assumed that the actual projected pixel coordinate $\boldsymbol{p}_i=(u_{p_i},v_{p_i})$ of point $\boldsymbol{P}_i$ on the calibration board, and the pixel coordinate $\boldsymbol{p}_i'=(u'_{p_i},v'_{p_i})$ obtained by reprojection. Among them, the reprojection coordinates are calculated in reverse according to Eq. (3) based on the obtained $\boldsymbol{H}_{p_i}$ and known $\boldsymbol{P}_i$ plane coordinates. The calculation formula is

$$\begin{cases} u'_{p_i}=\dfrac{h_{11}X_{P_i}^{\mathrm{W}}+h_{12}Y_{P_i}^{\mathrm{W}}+h_{13}}{h_{31}X_{P_i}^{\mathrm{W}}+h_{32}Y_{P_i}^{\mathrm{W}}+h_{33}}, \\ v'_{p_i}=\dfrac{h_{21}X_{P_i}^{\mathrm{W}}+h_{22}Y_{P_i}^{\mathrm{W}}+h_{23}}{h_{31}X_{P_i}^{\mathrm{W}}+h_{32}Y_{P_i}^{\mathrm{W}}+h_{33}}. \end{cases} \tag{12}$$

Then the reprojection error of point $\boldsymbol{P}_i$ and the reprojection error of the image are

$$\Delta e_i=\left\| \boldsymbol{p}_i-\boldsymbol{p}_i' \right\|_2=\sqrt{(u_{p_i}-u'_{p_i})^2+(v_{p_i}-v'_{p_i})^2}, \tag{13}$$

$$RMSE=\sqrt{\frac{1}{N}\sum_{i=1}^{N}\Delta e_i^2}=\sqrt{\frac{1}{N}\sum_{i=1}^{N}\left\| \boldsymbol{p}_i-\boldsymbol{p}_i' \right\|_2^2}. \tag{14}$$

Step 7 The cycle threshold η is set. If the specified cycle threshold is reached, the sequence solution of the optimal chromosome is returned, otherwise steps 4 to 6 are looped. The average fitness obtained in this evolution process is compared with the average fitness obtained in the last evolution process. If the ratio of the absolute value of the difference to the average fitness obtained in the last evolution is less than η, the cycle can be ended. This η is usually a priori value, and here it is taken as 0.05. The above ratio calculation formula is

$$\eta_i=\frac{\left| f_{\mathrm{avg}}-f_{\mathrm{LASTAVG}} \right|}{f_{\mathrm{LASTAVG}}}, \tag{15}$$

where f_{avg} is the average fitness value obtained in this evolution, f_{LASTAVG} is the average fitness value obtained in the previous evolution, and η_i is the calculated ratio result. In addition, for the rationality of the algorithm implementation, a maximum iteration number threshold k is set to limit the number of iterations of the algorithm.

Step 8 The optimal homography matrix is got. In the optimal chromosome sequence solution, the chromosome with the smallest fitness is taken as the optimal point pair sequence, and its corresponding homography matrix is the optimal homography matrix $\boldsymbol{H}$ between the calibration board and its image. The specific algorithm implementation steps can be seen in Fig.5.

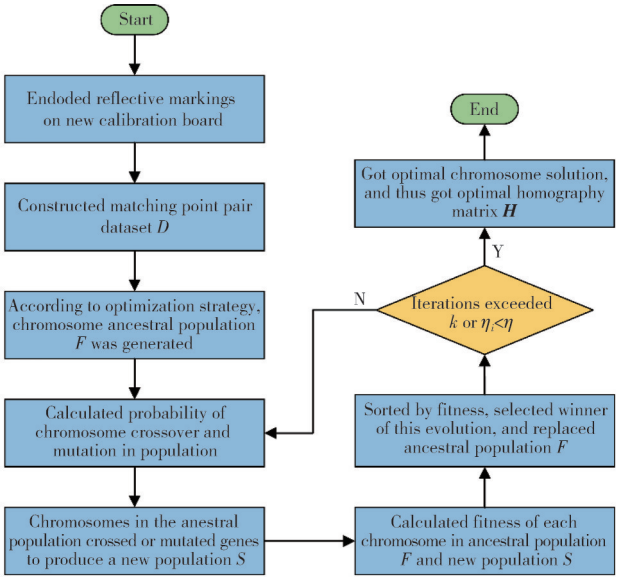

Fig. 5 AGA estimation *H* matrix flow chart

3 Experiments and results

The camera used in this article is an industrial camera, the camera type is an area-array camera, with a resolution of 2 592×1 944, a pixel size of 2.2 μm, a lens focal length of 12 mm, and the output image is of black and white type.

Firstly, a comparison experiment of the homography matrix estimation was conducted. Compared with the traditional estimation method, the proposed estimation method was improved in terms of image reprojection error and algorithm running time. Then, a camera calibration experiment was conducted, and the calibration results of several estimation algorithms were compared. This comparison demonstrated the reliability and effectiveness of the proposed method in camera calibration.

3.1 Comparative experiment of homography matrix estimation

First, the camera was fixed on a tripod to ensure that it was stable during shooting. Second, 15 positions were selected randomly in front of the camera's field of view and make sure that these positions were at different viewing angles or distances of the camera. The new calibration board was placed in turn at these positions with different viewing angles or distances from camera. Third, the board was photographed at every position by using the camera to obtain a set of images, as shown in Fig. 6. z is used to represent the approximate depth distance between the calibration board and the camera.

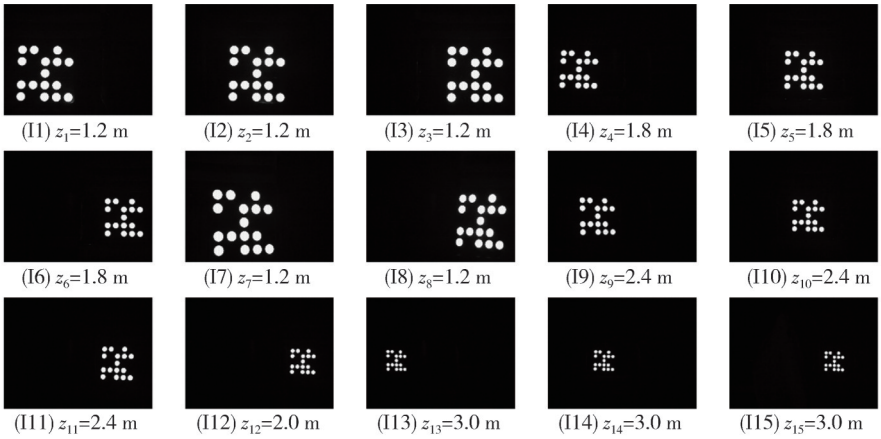

Fig. 6 Sequence of images captured by camera

After obtaining the image sequence, RANSAC, PROSAC, LMedS, and the adaptive genetic algorithm in this paper were used to calculate the homography matrix between each image and the calibration board plane, and the image reprojection error and algorithm running time were counted. The algorithm was used to calculate each image 100 times in a loop, and the average value was taken as the final result. This paper used RMSE as the standard for measuring the reprojection error. The calculation method is shown in Eqs. (13) and (14). In addition, to ensure the comparability of the four algorithms, the homography matrix iteration cutoff conditions of the four algorithms were kept consistent, with a maximum number of iterations $k=500$ or $\eta_i<0.05$.

Mean values of the four algorithms executed 100 times are shown in Fig. 7. It can be seen that the PROSAC algorithm, as an improvement on the RANSAC algorithm improves its computational execution efficiency, but its accuracy often decreases due to the narrowing of the selection range of matching point pairs in subsequent iterations. At the same time, it is limited by the influence of the initial model, and the final estimation accuracy might be very unsatisfactory, which is reflected in I5, I8, and I15 in Fig.7(a). The LMedS algorithm obtains the final model by comparing the median errors of the matching point pairs in the model before and after each iteration. Therefore, the

algorithm takes relatively more time to run and the accuracy can't reach the optimal level. The AGA optimized homography matrix algorithm proposed in this paper improves estimation accuracy and computational efficiency compared with the three traditional algorithms.

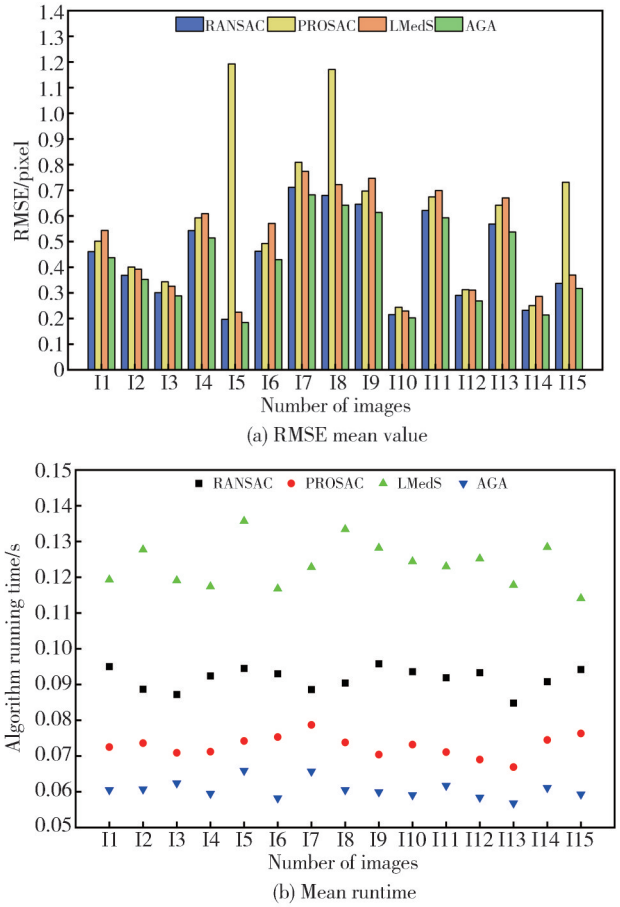

(a) RMSE mean value

(b) Mean runtime

Fig. 7 Mean values of four algorithms executed 100 times

I5, I8, and I15 in Fig.7 are excluded, and the impact of the initial model on PROSAC is ignored. Compared with the RANSAC algorithm, the reprojection error of the images is reduced by about 4.11%—7.85%, and the average running time of the algorithm decreases by about 25.85%—37.47%. Compared with the PROSAC algorithm, the reprojection error of the images is reduced by about 11.94%—16.91%, and the average running time of the algorithm decreases by about 11.99%—22.71%. Compared with the LMedS algorithm, the reprojection error of the images is reduced by about 10.19%—17.82%, and the average running time of the algorithm decreases by about 46.50%—53.35%.

3.2 Camera calibration comparison experiment

In order to verify the influence degree of the optimized homography matrix for camera calibration, the camera calibration comparison experiment was repeated 5 times. The homography matrix sequence calculated by different algorithms for the image sequence in Fig.6 was used for camera calibration using Zhang's calibration method[26]. The reprojection error of the image sequence obtained in the experiment and the time spent in completing the camera calibration were recorded. In the experiment, assuming that there are m images in the image sequence, the reprojection error of the image sequence is

$$ISRMSE = \frac{1}{m}\sum_{i=1}^{m} rmse_i, \tag{16}$$

where $ISRMSE$ represents the reprojection error of the image sequence, the reprojection error of any image is represented by $rmse_i$, and the subscript i indicates its position in the image sequence.

In addition, the entire camera calibration process included image preprocessing, key point detection, homography matrix calculation, Zhang's calibration method to calculate camera intrinsic parameters, etc. The specific results of the experiment are shown Fig.8.

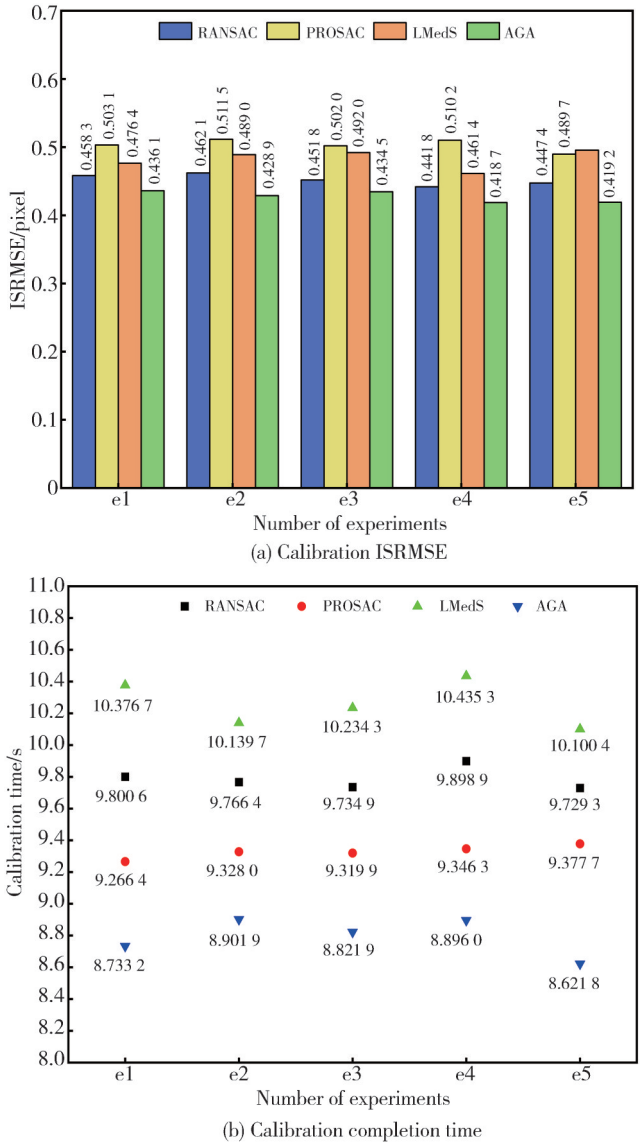

(a) Calibration ISRMSE

(b) Calibration completion time

Fig. 8 Camera calibration results of four algorithms

According to the results presented in Fig. 8, the homography matrix optimized by the adaptive genetic algorithm significantly improves in the accuracy and efficiency of camera calibration compared to the traditional algorithm. At the same time, the obtained results are consistent with the experimental results of homography matrix estimation mentioned above. In addition, this paper statistics the optimal camera intrinsic parameter matrix, the average reprojection error of the image sequence and the average camera calibration completion time obtained by the four algorithms in 5 repeated experiments, as shown in Table 1.

Table 1 Camera calibration results

Method	Camera matrix $\boldsymbol{K}$	Average reprojection error/pixel	Average calibration time/s
RANSAC	$\begin{bmatrix} 5\,902.876 & 0 & 1\,318.084 \\ 0 & 5\,901.323 & 967.538 \\ 0 & 0 & 1 \end{bmatrix}$	0.452 3	9.786 0
PROSAC	$\begin{bmatrix} 5\,899.049 & 0 & 1\,326.386 \\ 0 & 5\,897.731 & 956.390 \\ 0 & 0 & 1 \end{bmatrix}$	0.503 3	9.327 7
LMedS	$\begin{bmatrix} 5\,905.037 & 0 & 1\,313.029 \\ 0 & 5\,905.251 & 994.282 \\ 0 & 0 & 1 \end{bmatrix}$	0.482 9	10.257 3
AGA	$\begin{bmatrix} 5\,875.746 & 0 & 1\,310.413 \\ 0 & 5\,874.963 & 967.637 \\ 0 & 0 & 1 \end{bmatrix}$	0.427 5	8.795 0

It can be seen from Table 1 that in the camera intrinsic parameter matrix calculated by optimizing the homography matrix through the adaptive genetic algorithm, the camera's pixel principal point coordinates are closer to the real principal point coordinates. The focal lengths of the camera lens on the x axis and y axis is also closer to the real focal length. At the same time, during the camera calibration experiment, compared with the RANSAC, PROSAC, and LMedS algorithms, the AGA algorithm increases the average reprojection accuracy of the image sequence by 5.48%, 15.06%, and 11.47%, respectively; and the AGA algorithm improves the average completion time of camera calibration by 10.13%, 5.71%, and 14.26%, respectively.

It was evident that homography matrix optimization method based on adaptive genetic algorithm proposed in this paper improved the calculation accuracy and computing efficiency compared with traditional algorithms. This improvement was mainly due to the adaptive adjustment mechanism of algorithm parameters. During the evolution process, the cross rate and variability rate were dynamically adjusted according to the fitness changes of individuals (matching point pair sequences) in the population. In the early stage of evolution, higher initial cross-rate and variance rates enhanced population diversity and global search capabilities, thereby effectively avoided premature convergence to local optimal solutions. During the late stage of evolution, as the cross-rate and variance rates gradually decreased, evolution accelerated convergence to a more optimal solution or approximate solution. Throughout the process, this adaptive adjustment mechanism reduced the generation of redundant individuals, thereby reducing unnecessary calculations and improving the efficiency of calculations.

In addition, it must be noted that in the experiment, reprojection error was taken as an indicator of overall accuracy evaluation. However, the experiment includes multiple sources of error, such as feature extraction error, lens distortion error, and calculation error of the model. In this study, the impact of these errors was minimized by the key point extraction method of subpixel accuracy, the simplified distortion model, and the consistency of the number of data bits during the calculation process, thus ensuring the reliability of the comparison results of several algorithms.

4 Conclusions

A method to estimate the homography matrix was proposed based on an adaptive genetic algorithm to optimize the camera calibration process of Zhang's calibration method. First, the improved calibration board was placed in the camera field of view at different viewing angles to obtain a set of images. Then, two sets of comparison experiments were conducted, and RANSAC, PROSAC, LMedS, and the algorithm proposed in this paper were compared. Experimental results showed that compared with traditional algorithms, in terms of homography matrix estimation,

the algorithm in this paper could effectively improve the estimation accuracy and efficiency of the homography matrix. In terms of camera calibration, after adopting the algorithm in this paper, the accuracy estimation and calibration efficiency in the camera calibration process were also improved to a certain extent.

Acknowledgement

This work was supported by Anhui Province Key Research and Development Program (No.2022107020012).

Declaration of conflicting interests

The authors have no conflict of interests related to this publication.

References

[1] YANG S C, WEN J, WU S W, et al. Camera calibration with active standard Gaussian stripes for 3D measurement. Measurement, 2024, 233: 114793.

[2] ROMANO R, MAGGI D, HIROSE T, et al. Impact of lane keeping assist system camera misalignment on driver behavior. Journal of Intelligent Transportation Systems, 2021, 25(2): 157-169.

[3] BELL J J, MICARONI V, STRANO F, et al. Testing the impact of Remotely Operated Vehicle (ROVs) camera angle on community metrics of temperate mesophotic organisms: a 3D model-based approach. Ecological Informatics, 2023, 76: 102041.

[4] YU Y W, WANG K, DU L Q, et al. Matching point pair optimization registration method for point cloud model. Optics and Precision Engineering, 2023, 31(4): 503-516.

[5] LEE J, PARK E, YOO S. Multi-scale local implicit keypoint descriptor for keypoint matching//2023 IEEE/CVF Conference on Computer Vision and Pattern Recognition Workshops, June 17-24, 2023, Vancouver, BC, Canada. New York: IEEE, 2023: 6145-6154.

[6] DUAN Y, YU Y L, LIANG M Y. A weighted camera calibration algorithm with global solution of homography. Optics & Laser Technology, 2024, 174: 110585.

[7] FISCHLER M A, BOLLES R C. Random sample consensus: a paradigm for model fitting with applications to image analysis and automated cartography. Readings in Computer Vision, 1987: 726-740.

[8] CHUM O, MATAS J. Matching with PROSAC-progressive sample consensus//2005 IEEE Computer Society Conference on Computer Vision and Pattern Recognition, June 20-25, 2005, San Diego, CA, USA. New York: IEEE, 2005: 220-226.

[9] WANG Y, WANG J Y, DU W H, et al. Point cloud plane fitting algorithm based on least square median. Laser & Optoelectronics Progress, 2023, 60(4): 247-254.

[10] LAI H J, MENG X Y, XIAO S D, et al. Homography matrix estimation optimization algorithm based on RANSAC. Transducer and Microsystem Technologies, 2023, 42(8): 135-138.

[11] ZHAO C Y, ZHAO H C. Accurate and robust feature-based homography estimation using HALF-SIFT and feature localization error weighting. Journal of Visual Communication and Image Representation, 2016, 40: 288-299.

[12] HORVÁTH L, RICE G, ZHAO Y Q. Change point analysis of covariance functions: a weighted cumulative sum approach. Journal of Multivariate Analysis, 2022, 189: 104877.

[13] TORR P H S, ZISSERMAN A. MLESAC: a new robust estimator with application to estimating image geometry. Computer Vision and Image Understanding, 2000, 78(1): 138-156.

[14] RAHDAN A, BOLANDI H, ABEDI M. Design of on-board calibration methods for a digital Sun sensor based on Levenberg-Marquardt algorithm and Kalman filters. Chinese Journal of Aeronautics, 2020, 33(1): 339-351.

[15] YAN N, MEI Y P, YANG T, et al. RTHEN: Unsupervised deep homography estimation based on dynamic attention for repetitive texture image stitching. Displays, 2024, 82: 102670.

[16] VADIGI S, SETHI K, MOHANTY D, et al. Federated reinforcement learning based intrusion detection system using dynamic attention mechanism. Journal of Information Security and Applications, 2023, 78: 103608.

[17] WANG X Q. Research on image stitching technology based on deep learning. Beijing: Beijing University of Posts and Telecommunications, 2023.

[18] ZHANG Z, KANG J H, SUN Z F, et al. An optimization measurement method of laser sensor based on perspective projection model. Optics Communications, 2022, 506: 127582.

[19] XIONG K, HE X R, WANG C X, et al. Calibration method of fisheye camera for high-precision collimation measurement. Infrared and Laser Engineering, 2024, 53(2): 117-127.

[20] YIN Y H, GAO D, DENG K N, et al. Vision-based autonomous robots calibration for large-size workspace using ArUco map and single camera systems. Precision Engineering, 2024, 90: 191-204.

[21] WANG Y P, CUI X W, LI Y. Research on radar grid coordinates and optical pixel coordinate mapping method based on unisometric transformation. Journal of Signal Processing, 2023, 39(7): 1233-1242.

[22] HUANG L, ZHANG Q C, ASUNDI A. Camera calibration with active phase target: improvement on feature detection and optimization. Optics Letters, 2013, 38(9): 1446-1448.

[23] XU Y J, GAO F, ZHANG Z H, et al. A calibration method for non-overlapping cameras based on mirrored absolute phase target. The International Journal of Advanced Manufacturing Technology, 2019, 104(1): 9-15.

[24] MAHMOUDINAZLOU S, KWON C. A hybrid genetic

algorithm for the Min-max multiple traveling salesman problem. Computers & Operations Research, 2024, 162: 106455.
[25] MEI Z, GONG J C, GAO Y C, et al. Integrated optimization of structure and control systems based on a modified adaptive multi-population genetic algorithm. Journal of Central South University (Science and Technology), 2024, 55(2): 799-809.
[26] ZHANG Z. Flexible camera calibration by viewing a plane from unknown orientations//7th IEEE International Conference on Computer Vision, September 20-27, 1999, Kerkyra, Greece. New York: IEEE. 1999: 666-673.

基于自适应遗传算法的单应性矩阵估计方法

钱 程, 朱志峰*, 杨 科, 张 涛, 纪国泰

安徽工业大学 安徽省高校电力电子与运动控制重点实验室, 安徽 马鞍山, 243000

摘 要: 在相机标定中, 精确估计标定板世界坐标与其图像坐标之间的单应性矩阵是相机内参数高精度标定的关键步骤。现有的单应性矩阵估计方法存在依赖阈值、计算效率低、初始模型或排序质量影响结果等问题。本文提出了一种基于自适应遗传算法的单应性矩阵估计方法。首先, 设计了一种新型的圆形网格标定板, 并优化了匹配点对数据集初次抽样的策略。然后, 根据自适应遗传算法建立估计单应性矩阵的数学模型, 从而获得标定板与其图像之间的最优单应性矩阵。最后, 结合张氏标定法计算出相机内参数。实验结果表明: 基于自适应遗传算法的估计方法与传统的估计方法RANSAC、PROSAC和LMedS相比, 图像的重投影误差分别降低约4.11%－7.85%, 11.94%－16.91%, 10.19%－17.82%。算法的平均运行时间分别减少约25.85%－37.47%, 11.99%－22.71%, 46.50%－53.35%。另外, 将本文的单应性矩阵估计方法应用于相机的标定过程中, 对比结果显示: 该方法相比较于传统方法, 相机在标定过程中的平均精度分别提高约5.48%, 15.06%, 11.47%。相机的平均标定效率分别提升约10.13%, 5.71%, 14.26%。本文提出的单应性矩阵估计方法不仅能够得到可靠的结果, 而且对提升相机标定过程中的估计精度和计算效率方面具有一定的价值和意义。

关键词: 相机标定; 相机内参; 标定板; 单应性矩阵; 重投影误差 ;张氏标定

引用格式: QIAN Cheng, ZHU Zhifeng, YANG Ke, et al. Homography matrix estimation method based on adaptive genetic algorithm. Journal of Measurement Science and Instrumentation, 2025, 16(4): 558-568. DOI: 10.62756/jmsi.1674-8042.2025054